Original Research Article

Dementia
and Geriatric
Cognitive Disorders

Dement Geriatr Cogn Disord 2001;12:78–84

Accepted: April 26, 2000

Age-Related Changes in Energy Production in Fresh Senescence-Accelerated Mouse Brain Slices as Revealed by Positron Autoradiography

Naoto Omata[a,b] Tetsuhito Murata[a,b] Yasuhisa Fujibayashi[a] Atsuo Waki[a]
Norihiro Sadato[a] Mitsuyoshi Yoshimoto[a] Yuji Wada[b]
Yoshiharu Yonekura[a]

[a]Biomedical Imaging Research Center and [b]Department of Neuropsychiatry, Fukui Medical University, Fukui, Japan

Key Words

Brain slice · Energy production · Glucose metabolism · Senescence-accelerated mouse · Glycolytic capacity · Mitochondrial function · O_2 deprivation · 2,4-Dinitrophenol

Abstract

To investigate age-related changes in cerebral energy production, we compared senescence-accelerated prone mice (SAMP8) as an animal model of accelerated aging and senescence-accelerated resistant mice (SAMR1) as a control. Considering that the cerebral glucose metabolic rate (CMRglc) at the time of O_2 deprivation and 2,4-dinitrophenol (DNP) loading would reflect anaerobic glycolytic capacity and mitochondrial function, respectively, we investigated dynamic changes in CMRglc before and after loading with these perturbations. Fresh brain slices were incubated with [^{18}F]2-fluoro-2-deoxy-*D*-glucose ([^{18}F]FDG) in oxygenated Krebs-Ringer solution at 36°C, and serial two-dimensional time-resolved images of [^{18}F]FDG uptake in these slices were obtained on the imaging plates. The fractional rate constant (=k_3*) of [^{18}F]FDG proportional to the CMRglc was evaluated by applying the Gjedde-Patlak graphical method to the image data. The k_3* value before the hypoxic perturbation in all of the brain sites analyzed was higher in SAMP8 than SAMR1 in both the 2- and 10-month-old groups. With O_2 deprivation, k_3* values were higher without site specificity in the 2-month-old SAMP8 than in 2-month-old SAMR1, whereas in 10-month-old mice, there was no significant difference between the two groups. In contrast, with DNP loading, while no significant difference was noted between 2-month-old SAMP8 and 2-month-old SAMR1, in 10-month-old mice, the SAMP8 group showed lower values in certain regions than SAMR1 mice. These results suggest that in the brain tissue of SAMP8, a marked transient enhancement of anaerobic glycolytic capacity in the 2-month-olds and a decrease in mitochondrial function in the subsequent period occur, as a result of which glucose metabolism appears to be enhanced in both the 2- and 10-month-old groups compared to SAMR1 mice.

Introduction

The intracerebral concentration of ATP, which is an essential energy source for cellular functions, decreases with age [1]. To investigate age-related changes in mitochondrial function and in glycolysis, which produces

KARGER

Fax + 41 61 306 12 34
E-Mail karger@karger.ch
www.karger.com

1420–8008/01/0122–0078$17.50/0

Accessible online at:
www.karger.com/journals/dem

Tetsuhito Murata, MD, PhD
Department of Neuropsychiatry, Fukui Medical University
Matsuoka-cho, Fukui 910-1193 (Japan)
Tel. +81 776 61 3111, ext 2321, Fax +81 776 61 8136
E-Mail tmurata@fmsrsa.fukui-med.ac.jp

ATP, it is useful to measure glucose metabolism while interrupting some of the metabolic pathways of a series of energy production mechanisms. When O_2 deprivation is imposed, anaerobic energy production compensates for the lack of energy, at which time the glucose requirement reflects anaerobic glycolytic capacity [2, 3]. Also, with 2,4-dinitrophenol (DNP) loading, respiration within the mitochondria occurs, but ATP is not produced, so glucose uptake increases to the extent of compensating for the ATP produced in the mitochondria, thereby reflecting mitochondrial function [4, 5].

The senescence-accelerated mouse (SAM), an animal model of accelerated aging, was established by Takeda et al. [6, 7]. SAM consists of two strains, the senescence-accelerated prone mouse (SAMP), which after normal growth shows signs of aging such as a rapid decrease in activity, hair loss and loss of sheen, and achieves a mean lifespan of less than 1 year. The other is the senescence-accelerated resistant mouse (SAMR), which shows normal signs of aging. SAMP8, which is a substrain of SAMP, is recognized as an animal model of senile dementia because it exhibits gradually deteriorating cerebral functional impairment, in particular decreased memory and learning ability, after the age of 2 months [8, 9]. Regarding age-related changes in energy production mechanisms in SAM, previous studies have focused on isolated mitochondrial function [4, 10] or dissociated cell glucose uptake [11]. However, the interaction between glycolysis and mitochondrial function and their compensatory mechanisms has not yet been adequately evaluated.

In experimental systems in which fresh brain slices are immersed in artificial medium for prolonged periods, alteration of the external environment, namely the composition of the medium solution or oxygen supply, makes it easy to impose various perturbations such as O_2 deprivation or DNP loading. As an imaging technique in living brain slices, we recently developed the 'dynamic positron autoradiography technique' (dPAT), which utilizes positron-emitter-labeled tracers as a probe and an imaging plate as the detector [12, 13]. Owing to the highly specific radioactivity of the radiotracers, high energy of positrons and high sensitivity of the imaging plate, this technique allows the quantitative construction of serial two-dimensional images of radioactivity in the slices with a short exposure time while the brain tissue is still alive in the incubation solution.

In the present study, we used dPAT with [^{18}F]2-fluoro-2-deoxy-*D*-glucose ([^{18}F]FDG) and fresh brain slices to determine how brain anaerobic glycolytic capacity and mitochondrial function change with age by comparing SAMP8, an animal model of accelerated aging, with SAMR1 as a control. By imposing O_2 deprivation and DNP loading, dynamic changes in the cerebral glucose metabolic rate (CMRglc) before and after these perturbations were quantitatively evaluated by applying the Gjedde-Patlak graphical method [14, 15] to the image data.

Materials and Methods

Preparation of Brain Slices and Setup for Incubation

Two- and 10-month-old male SAMP8 and SAMR1 were used. The animals were bred under standard conditions, housed at 24 ± 1 °C and allowed free access to food and water; the light-dark cycle was set to 12 h. After decapitation, the brains were quickly removed and immersed in oxygenated, cooled (1–4 °C) Krebs-Ringer solution (composition, m*M*: NaCl, 124; KCl, 5; $MgCl_2$, 1; $CaCl_2$, 2; KH_2PO_4, 1.2; $NaHCO_3$, 26; glucose, 10). Sagittally sectioned brain slices, 300 μm thick, were prepared with a microslicer (DTK-2000; Dosaka EM, Kyoto, Japan) and incubated in double polystyrene chambers (outer and inner chambers) as previously described [13]. A side view of this setup is illustrated in figure 1. Briefly, the bottom of the outer and inner chambers was cut to make a rectangular hole, over which a transparent polyvinylidene chloride film (10 μm thick) or a fine nylon net (80 μm thick) was tightly stretched and fixed in place by gluing to the side wall. The outer chamber was filled with 80 ml of Krebs-Ringer solution (to a depth of 8 mm) in which the inner chamber having numerous small holes (4 mm in diameter) on the side wall was immersed. Brain slices were arranged on the nylon net of the inner chamber and were lightly fixed in place by covering with another fine nylon net, which was stretched and glued to the upper side of a 300-μm-thick stainless steel ring (2 cm in inner diameter). The bathing solution was kept at 36 °C and continuously bubbled with 95% O_2/5% CO_2 gas supplied through a fine silicone tubing introduced into the inner chamber at six sites, to promote consistent perfusion within the chamber. O_2 deprivation was induced by replacing O_2 with N_2 in the gas phase of the chamber. A Blood Gas System 280 (Ciba Corning Diagnostics Corp., Medfield, Mass., USA) was used to serially measure O_2 partial pressure in several experiments. Values were 20–25 and 650–700 mm Hg, respectively, when 95% N_2/5% CO_2 gas and 95% O_2/5% CO_2 gas were used. DNP was obtained from Nacalai Tesque Co. (Kyoto, Japan).

Production of Radiotracer and Measurement of [^{18}F]FDG Uptake

[^{18}F]FDG with specific radioactivity of 1–2 Ci/mmol was synthesized by the method of Hamacher et al. [16] with an automated [^{18}F]FDG synthesis system (NKK Co. Ltd., Tokyo, Japan). Total concentration (labeled plus unlabeled) used in this study ranged from 0.43 to 1.12 μg/ml (2.3–6.1 μ*M*). After 1 h preincubation of brain slices in Krebs-Ringer solution at 36 °C (pH 7.3–7.4), the inner chamber containing the slices was removed and put into another outer chamber in which [^{18}F]FDG had been diluted at 150 kBq/ml with prewarmed Krebs-Ringer solution. A set of 4 double polystyrene chambers each containing 12 slices was placed on an imaging plate (BAS-MP 2040S, Fuji Photo Film Co., Japan), which was replaced with a new plate every 10 min. The exposed imaging plates were

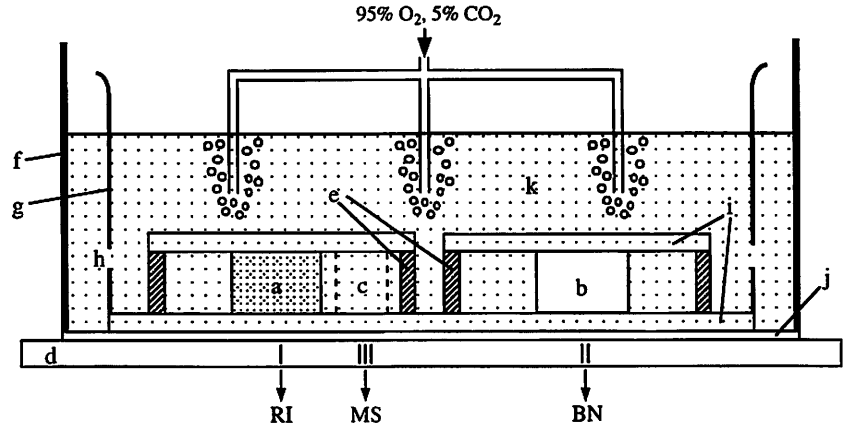

Fig. 1. Schematic side view of the setup for incubation and detection of radioactivity signal on the imaging plate. a = Brain slice (300 μm thick); b = nylon sheet (300 μm thick); c = 300-μm-thick bathing solution layer; d = imaging plate; e = stainless steel ring; f = outer chamber; g = inner chamber; h = hole in the side wall of the inner chamber; i = nylon net (80 μm thick); j = polyvinylidene chloride film (10 μm thick); k = Krebs-Ringer solution containing [^{18}F]FDG. For simplification, scaling is arbitrary.

scanned with a bio-imaging analyzer (BAS-1500, Fuji Photo Film Co.) and the images displayed on a Macintosh computer at a pixel size of 100 μm.

Calculation of CMRglc and Gjedde-Patlak Graphical Analysis

The three-compartment model for [^{18}F]FDG using brain slices is based on the distribution of [^{18}F]FDG in bathing medium [Cp*(t)], [^{18}F]FDG in brain tissue [Ce*(t)], and [^{18}F]FDG-6-PO_4 in brain tissue [Cm*(t)] [17, 18]. First-order rate constants describing transport between the compartments include K_1* and k_2* for forward and reverse [^{18}F]FDG transport, and k_3* and k_4* for phosphorylation of [^{18}F]FDG and dephosphorylation of [^{18}F]FDG-6-PO_4. In the equilibrium condition, on the basis that the influx constant of [^{18}F]FDG [= K_1*k_3*/(k_2* + k_3*)] is equivalent to the rate of [^{18}F]FDG-6-PO_4, CMRglc can be estimated with the following expression [19]:

$$CMRglc = Cp/LC \cdot (K_1^* k_3^*/(k_2^* + k_3^*)) = Cp/LC \cdot K \quad (1)$$

where Cp is the medium glucose concentration and LC is the lumped constant, which accounts for differences in the transport and phosphorylation of [^{18}F]FDG and glucose [18–20]. K is the macroparameter for the net influx constant of [^{18}F]FDG. If both Cp and LC are constant, a linear relationship should be maintained between K and CMRglc according to equation 1, and thus K itself can be considered an index of CMRglc. The Gjedde-Patlak graphical method [14, 15] employed to determine the macroparameter K was based on the following equation:

$$Ci^*(t)/Cp^*(t) = K \cdot \int_0^t Cp^*(\tau)d\tau/Cp^*(t) + V \quad (2)$$

where Ci*(t), representing the sum of Ce*(t) and Cm*(t), is the total brain tissue radioactivity, Cp*(t) is the input function and V is related to the effective distribution volume of the tracer [^{18}F]FDG. Thus, assuming that k_4* is equal to zero, K was estimated from the slope of the linear portion of the graph, Ci*(t)/Cp*(t) (vertical y axis) versus

$$\int_0^t Cp^*(\tau)d\tau/Cp^*(t)$$ (horizontal x axis).

Here, when brain slices are incubated in a medium of fixed FDG concentration without interference from blood-borne factors, the rate of delivery of the tracer to the slices is determined by the diffusion rate rather than the product of the cerebral perfusion rate and extraction fraction, as in the living brain. Therefore, the slope of the ratio of Ci*(t)/Cp*(t) as a function of

$$\int_0^t Cp^*(\tau)d\tau/Cp^*(t)$$

does not have the units of the net influx constant defined by Gjedde-Patlak (K, ml · g^{-1} · min^{-1}) but is rather a fractional rate constant (k_3*, min^{-1}), proportional to the rate constant for hexokinase activity in the brain slices. Moreover, the lumped constant does not retain its normal meaning in the present study, as there is no ratio of blood-brain permeability of FDG and glucose, but only the ratio of the affinities of hexokinase for FDG and glucose.

Defining RI (I in fig. 1) as the radioactivity signal (photostimulated luminescence, PSL/mm^2) on the imaging plate detected beneath the brain region of interest (a in fig. 1), BN (II in fig. 1) as the radioactivity signal on the imaging plate detected beneath the nylon sheet (b in fig. 1, 300 μm thick, specific gravity = 1.14) as a slice phantom for measuring the background noise and MS (III in fig. 1) as the average radioactivity signal on the imaging plate detected at 4 places beneath the bathing medium solution (c in fig. 1, 300 μm thick) surrounding each brain slice or nylon sheet, the proportion of the radioactivity signal contributed by either the 300-μm-thick brain tissue or 300-μm-thick bathing solution layer can be calculated from RI minus BN and MS minus BN, respectively, since the radioactivity signal from the 300-μm-thick nylon sheet is 0. Here, the same amount of [^{18}F]FDG either in a 300-μm-thick brain slice or in a 300-μm-thick bathing solution layer (the densities of which are nearly equal) should yield the same amount of signal on the imaging plate. Thus, Ci*(t)/Cp*(t) can be expressed in terms of the following ratio:

$$Ci^*(t)/Cp^*(t) = (RI - BN)/(MS - BN) \quad (3)$$

Here, the linearity of the response of the imaging plates (PSL/mm^2) to the radioactivity (Bq/ml) was checked for BN, MS and MS–BN

(data not shown). In all three, regression lines passing close to the original points could be fitted, with all the data presented here within the respective linear range.

The real radioactivity signal of MS-BN decreased exponentially with time from the start of incubation. When decay corrected, however, it showed an almost constant signal throughout the time course (data not shown). Thus, Ci*(t)/Cp*(t) (vertical y axis) at each time point calculated above was plotted against real time (horizontal x axis) indicating

$$\int_0^t Cp^*(\tau)d\tau/Cp^*(t)$$ (as the mean value of 24 slices).

Time zero (t = 0) is defined as the point at which [^{18}F]FDG was introduced into the bathing medium containing the brain slices. As shown in figure 2, for example, Ci*(t)/Cp*(t) within the initial part (from 0 to 30 min) of each plot did not show a linear relationship with time, indicating an approach to equilibrium between the incubation medium and the interstitial fluid of the brain slices. Thereafter, the Ci*(t)/Cp*(t) of the unloaded control showed a linear relationship with time (linear regression coefficient $r>0.98$, from 40 to 240 min), indicating constant glucose utilization (data not shown). When the bathing medium was subjected to exogenous perturbations (O_2 deprivation/DNP loading), it took 20–30 min before a new equilibrium state was reached, with this temporary phase manifested as a transient curve. To evaluate the dynamic changes in regional CMRglc before and after loading of these perturbations, the slopes ($=k_3^*$) were calculated separately from the Gjedde-Patlak plot under each equilibrium state for 60 min in the preloading (from 70 to 130 min) and postloading (from 30 min after the end of O_2 deprivation/DNP loading) phases using linear regression analysis.

Statistical Analysis

The images were analyzed using the software MacBAS version 2 (Fuji Photo Film Co.) developed for the Macintosh computer. The presented values are shown as the mean ± SEM of a total of 24 slices from 6 mice obtained in 3 experiments. The Mann-Whitney U test was used to evaluate the significance of differences.

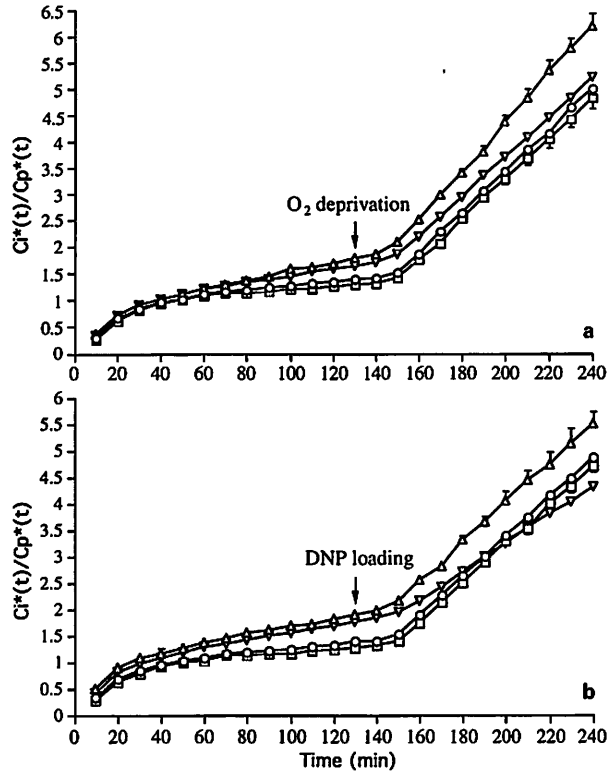

Fig. 2. Effect of O_2 deprivation (**a**) and DNP loading (**b**) on the Gjedde-Patlak plots of [^{18}F]FDG uptake in the frontal cortex: 2-month-old SAMR1 (○), 2-month-old SAMP8 (△), 10-month-old SAMR1 (□) and 10-month-old SAMP8 (▽). Addition of O_2 deprivation or DNP loading is indicated by arrows. Values are means ± SEM (SEM is shown for only the upper- and lowermost lines).

Results

Figure 2a shows the Gjedde-Patlak plots in the frontal cortex when 2- and 10-month-old SAMP8 and SAMR1 brain slices were subjected to O_2 deprivation, and figure 2b those in the frontal cortex when DNP (100 μ*M*) loading was imposed. Prior to O_2 deprivation or DNP loading, the fractional rate constant ($=k_3^*$) of [^{18}F]FDG in both the 2- and 10-month-old groups showed higher values in SAMP8 than in SAMR1.

With O_2 deprivation, k_3^* values increased dramatically. However, in 2-month-old SAMP8 and SAMR1 subjected to O_2 deprivation, k_3^* values remained higher in the former than in the latter compared with prior to O_2 deprivation, whereas in 10-month-old mice, there was no significant difference between the two groups. The results in each of the four analyzed sites are listed in table 1.

As with O_2 deprivation, k_3^* values also increased dramatically with DNP loading. Although there was no significant difference in this value between the 2-month-old SAMP8 mice and SAMR1 mice, 10-month-old SAMP8 mice showed lower values particularly in the frontal cortex, caudate putamen and cerebellum than the 10-month-old SAMR1 group. In the thalamus, however, no significant difference was noted between the two groups. The results in each of the four analyzed sites are listed in table 2.

Discussion

The increase in the fractional rate constant ($=k_3^*$) of [^{18}F]FDG induced by O_2 deprivation is thought to reflect compensation by anaerobic glycolytic capacity for the

Table 1. Effect of O_2 deprivation loading on the fractional rate constant of [^{18}F]FDG

Brain region		2 months old		10 months old	
		SAMR1	SAMP8	SAMR1	SAMP8
Frontal cortex	Preloading	3.67±0.31	7.26±0.35*	3.35±0.33	6.50±0.36*
	Postloading	39.60±2.47	47.48±2.42*	36.42±2.53	38.48±2.32
Caudate putamen	Preloading	4.29±0.69	8.57±0.87*	4.12±1.12	7.11±0.85*
	Postloading	50.84±6.90	64.17±7.20*	48.87±8.23	52.31±6.98
Thalamus	Preloading	5.71±1.10	9.28±0.65*	5.21±0.58	7.14±1.32*
	Postloading	50.09±5.32	66.67±6.51*	45.67±5.36	51.76±4.57
Cerebellum	Preloading	2.86±0.68	5.02±0.65*	2.98±0.78	4.96±0.72*
	Postloading	11.68±3.36	16.67±5.20*	10.50±5.54	12.27±4.81

* $p < 0.05$; significantly different from SAMR1 of the same age. The k_3* (×1,000), indicating the fractional rate constant of [^{18}F]FDG, was obtained from the slope of the regression equation (y = ax + b) fitted to Gjedde-Patlak plots using the linear regression analysis. y = Ci*(t)/Cp*(t) expressed in terms of the radioactivity signal ratio [= (RI–BN)/(MS–BN)] by equation 3 (see text); x = time (min) after the start of incubation; a = slope of the line, b = intercept. All values are means ± SEM obtained from 24 slices.

Table 2. Effect of DNP loading on the fractional rate constant of [^{18}F]FDG

Brain region		2 months old		10 months old	
		SAMR1	SAMP8	SAMR1	SAMP8
Frontal cortex	Preloading	3.38±0.34	6.68±0.31*	3.08±0.36	6.00±0.33*
	Postloading	36.14±1.66	38.62±4.16	37.45±1.22	26.94±3.58*
Caudate putamen	Preloading	4.31±1.31	8.47±0.99*	4.10±0.57	7.22±1.01*
	Postloading	52.81±7.14	54.67±6.69	56.30±6.87	42.23±5.55*
Thalamus	Preloading	5.34±2.35	8.99±2.01*	4.87±1.87	7.26±1.98*
	Postloading	52.37±3.80	55.40±4.79	54.17±5.61	53.22±6.38
Cerebellum	Preloading	2.84±0.65	5.17±0.54*	2.84±1.45	5.09±0.77*
	Postloading	12.91±1.42	13.36±2.30	13.53±2.57	9.16±1.97*

* $p < 0.05$; significantly different from SAMR1 of the same age. The k_3* (×1,000), indicating the fractional rate constant of [^{18}F]FDG, was obtained from the slope of the regression equation (y = ax + b) fitted to Gjedde-Patlak plots using the linear regression analysis as described in the legend of table 1. All values are means ± SEM obtained from 24 slices.

energy insufficiency associated with respiratory inhibition [3]. Accordingly, the finding that k_3* values in 2-month-old SAMP8 mice on O_2 deprivation were higher than those of age-matched SAMR1 mice suggests that anaerobic glycolytic capacity is enhanced in the former group compared to the latter. However, the fact that no significant difference was found in the 10-month-old groups indicates that anaerobic glycolytic capacity is not enhanced in SAMP8 10-month-olds, and that this capacity can be regarded as a transient phenomenon occurring in the course of aging. These findings are also consistent with those reported by Sato et al. [11], stating that the glucose transporter protein in the cerebral cortex is transiently overproduced in 1- to 2-month-old SAMP8.

As oxidative phosphorylation, together with glycolysis, constitute the process of energy producing glucose metabolism, it is conceivable that glucose metabolism and mitochondrial function interact with each other. When changes in glucose metabolism are found, it is important to investigate to what extent mitochondrial function has contributed to those changes. O_2 deprivation and DNP loading differ with respect to the presence or absence of

substrate flow in the electron transport system. With O_2 deprivation, the TCA cycle is blocked [2], preventing the flow of substrate in the electron transport system [21]. In contrast, when DNP, an uncoupler, is loaded, a state is created in which substrate flows in the electron transport system and respiration occurs, but ATP is no longer produced [5]. This state is more marked in the higher mitochondrial function [4], and as a result ATP production comes to depend on glycolysis. Accordingly, the greater the increase in k_3* value at the time of DNP loading, the higher the original mitochondrial function can be considered to be. In the present study, although there was no significant difference noted in k_3* value with DNP loading between the 2-month-old SAMP8 and SAMR1 mice, in the 10-month-old mice, the SAMP8 group showed lower values particularly in the frontal cortex, caudate putamen and cerebellum than the SAMR1 group. Accordingly, mitochondrial function in SAMP8, particularly in these brain regions, is thought to gradually decline with age. However, the thalamus differed in this respect from the other three sites, with no significant differences seen in k_3* values between 10-month-old SAMP8 and SAMR1 even after DNP loading. An age-related decline in SAMP8 mitochondrial function has previously been reported [4, 10], although in these studies mitochondria were obtained from homogenized liver and whole brain. As far as we are aware, the present study using dPAT is the first to demonstrate a site specificity in this decline in mitochondrial function.

These differences in changes in brain glucose metabolism in SAMP8 and SAMR1 in response to O_2 deprivation and DNP loading indicate that age-related changes in anaerobic glycolytic capacity and mitochondrial function in the central nervous system of SAMP8 are different. In 2-month-olds, in the absence of any perturbation, the higher K values noted in SAMP8 as compared to SAMR1 are considered to reflect a transient enhancement of anaerobic glycolysis in the former. This period, namely 2 months of age, in which this transient enhancement occurs immediately precedes the time at which the memory and learning disturbances characteristic of SAMP8 begin to become apparent. These results therefore suggest that changes in brain glucose metabolism develop prior to the appearance of dementia symptoms. However, in the present work, no obvious derangement of mitochondrial function was seen in 2-month-old SAMP8. Therefore, it was clear that anaerobic glycolytic capacity was enhanced independently, without being affected by mitochondrial function. With the age-dependent decline in oxidative phosphorylation capacity, the function of glycolysis as an ATP-generating pathway becomes vital [22]; in the SAMP8 studied here, as mitochondrial injury became apparent in the course of progressive aging, the degree of dependence on glycolysis as energy supply is thought to have increased. However, since the enhancement of anaerobic glycolytic capacity in 2-month-old SAMP8 is only a transient phenomenon no longer seen at 10 months, it cannot compensate for the severe mitochondrial injury present at this stage. Accordingly, we surmise that with the gradual progression of mitochondrial injury with age, compensatory mechanisms become increasingly less adequate in dealing with the resulting decrease in energy production, with this being responsible for the development of symptoms such as memory and learning impairment and decrease in activity. However, it is not clear at this stage whether these age-related changes in the energy production mechanisms are specific to SAMP8 mice or universally apply to the phenomenon of aging. Solving this problem will require molecular-level studies of age-related changes in the energy production mechanisms in SAMP8, and comparison with data obtained from studies of models other than SAM.

In summary, in the present study using dPAT, the brain tissue of SAMP8, an animal model of accelerated aging, showed transient enhancement of anaerobic glycolysis in 2-month-olds and a subsequent decline in mitochondrial function. These results suggest that, as compared with SAMR1, glucose metabolism in SAMP8 is enhanced at both 2 and 10 month of age.

Acknowledgments

This study was supported in part by a research Grant (JSPS-RFTF97L00203) from the 'Research for the Future' Program of the Japan Society for the Promotion of Science.

References

1 Ulfert G, Schmidt U, Hoyer S: Glucose and energy metabolism of rat cerebral cortex during aging. Exp Brain Res 1982;(suppl 5):102–111.
2 Matsuoka S, Jarmakani JM, Young HH, Uemura S, Nakanishi T: The effect of glutamate on hypoxic newborn rabbit heart. J Mol Cell Cardiol 1986;18:897–906.
3 Mercado CL, Loeb JN, Ismail-Beigi F: Enhanced glucose transport in response to inhibition of respiration in Clone 9 cells. Am J Physiol 1989;257:C19–C28.
4 Nakahara H, Kanno T, Inai Y, Utsumi K, Hiramatsu M, Mori A, Packer L: Mitochondrial dysfunction in the senescence accelerated mouse (SAM). Free Radic Biol Med 1998;24: 85–92.
5 Sibille B, Ronot X, Filippi C, Nogueira V, Keriel C, Leverve X: 2,4 Dinitrophenol-uncoupling effect on delta ψ in living hepatocytes depends on reducing-equivalent supply. Cytometry 1998;32:102–108.
6 Takeda T, Hosokawa M, Takeshita S, Irino M, Higuchi K, Matsushita T, Tomita Y, Yasuhira K, Hamamoto H, Shimizu K, Ishii M, Yamamuro T: A new murine model of accelerated senescence. Mech Ageing Dev 1981;17:183–194.
7 Takeda T, Hosokawa M, Higuchi K: Senescence-accelerated mouse (SAM): A novel murine model of senescence. Exp Gerontol 1997; 32:105–109.
8 Ohta A, Hirano T, Yagi H, Tanaka S, Hosokawa M, Takeda T: Behavioral characteristics of SAM-P/8 strain in Sidman active avoidance task. Brain Res 1989;498:195–198.
9 Okuma Y, Nomura Y: Senescence-accelerated mouse (SAM) as an animal model of senile dementia: Pharmacological, neurochemical and molecular biological approach. Jpn J Pharmacol 1998;78:399–404.
10 Nishikawa T, Takahashi JA, Fujibayashi Y, Fujisawa H, Zhu B, Nishimura Y, Ohnishi K, Higuchi K, Hashimoto N, Hosokawa M: An early stage mechanism of the age-associated mitochondrial dysfunction in the brain of SAMP8 mice; an age associated neurodegeneration animal model. Neurosci Lett 1998;254: 69–72.
11 Sato E, Inoue A, Kurokawa T, Ishibashi S: Early changes in glucose metabolism in the cerebrum of senescence accelerated mouse: Involvement of glucose transporter. Brain Res 1994;637:133–138.
12 Murata T, Waki A, Omata N, Fujibayashi Y, Sadato N, Yano R, Yoshimoto M, Isaki K, Yonekura Y: Dynamic changes in glucose metabolism by lactate loading as revealed by a positron autoradiography technique using rat living brain slices. Neurosci Lett 1998;249: 155–158.
13 Murata T, Omata N, Fujibayashi Y, Waki A, Sadato N, Yoshimoto M, Omori M, Isaki K, Yonekura Y: Dynamic changes in glucose metabolism induced by thiamine deficiency and its replenishment as revealed by a positron autoradiography technique using rat living brain slices. J Neurol Sci 1999;164:29–36.
14 Gjedde A: High- and low-affinity transport of D-glucose from blood to brain. J Neurochem 1981;36:1463–1471.
15 Patlak CS, Blasberg RG, Fenstermacher JD: Graphical evaluation of blood-to-brain transfer constants from multiple-time uptake data. J Cereb Blood Flow Metab 1983;3:1–7.
16 Hamacher K, Coenen HH, Stocklin G: Efficient stereospecific synthesis of no-carrier-added 2-[^{18}F]-fluoro-2-deoxy-*D*-glucose using aminopolyether supported nucleophilic substitution. J Nucl Med 1986;27:235–238.
17 Newman GC, Hospod FE, Patlak CS: Brain slice glucose utilization. J Neurochem 1988;51: 1783–1796.
18 Sokoloff L, Reivich M, Kennedy C, Des Rosiers MH, Patlak CS, Pettigrew KD, Sakurada O, Shinohara M: The [^{14}C]deoxyglucose method for the measurement of local cerebral glucose utilization: Theory, procedure, and normal values in the conscious and anesthetized albino rat. J Neurochem 1977;28:897–916.
19 Huang SC, Phelps ME, Hoffman EJ, Sideris K, Selin CJ, Kuhl DE: Noninvasive determination of local cerebral metabolic rate of glucose in man. Am J Physiol 1980;238:E69–E82.
20 Phelps ME, Huang SC, Hoffman EJ, Selin C, Sokoloff L, Kuhl DE: Tomographic measurement of local cerebral glucose metabolic rate in humans with (F-18)2-fluoro-2-deoxy-D-glucose: Validation of method. Ann Neurol 1979; 6:371–388.
21 Pastoris O, Dossena M, Foppa P, Arnaboldi R, Gorini A, Villa RF, Benzi G: Modifications by chronic intermittent hypoxia and drug treatment on skeletal muscle metabolism. Neurochem Res 1995;20:143–150.
22 Cimino M, Marini P, Colombo S, Cattabeni F, Bianchi M, Magnani M: Localization and age-dependent expression of hexokinase mRNA in the rat brain. Brain Res Mol Brain Res 1994; 25:1–6.